Universidad Nacional Autónoma de México

Programa de posgrado en Astrofísica
Instituto de Radioastronomía y Astrofísica

Recovering the star formation histories of galaxies using spectrophotometric analysis

PhD Project Update

PhD in Science (Astrophysics)

Author:
Mariana Rivas-Sánchez

Supervisors:
Dr. Jacopo Fritz, IRyA UNAM
Dr. Maarten Baes, Ghent University

Morelia, Mich. December 2023

1 Introduction

Galaxy spectra analysis provides a deep understanding of the properties and content of stars, gas, and dust within them. Among the most critical drivers of these properties, galaxy morphology and its total stellar mass are the dominant ones, and they often dictate the way stars are formed, i.e. the star formation history (SFH) and, hence, the spectral appearance (Kennicutt & Evans, 2012; Conselice, 2014) of galaxies.

Initial galaxy categorisation techniques involved direct visual observations of optical images, which gradually transitioned to more quantitative approaches -ranging from the Hubble diagram-based morphological classification (Hubble, 1926; de Vaucouleurs, 1959) to the use of parametric classification like colour-magnitude diagrams (Bell et al., 2003), the galactic main sequence (Brinchmann et al., 2004), and spectral classification (Sodré & Cuevas, 1994). Each classification aims to characterise the galaxy in terms of stellar populations, given that stellar evolution significantly influences galaxy evolution.

Stellar evolution is maybe the major driver of galaxy changes, and for over two decades, efforts have been made to reconstruct the SFH history of the Universe (Madau et al. 1996, 1998, Madau & Dickinson 2014). It is widely accepted that star formation activity was more prevalent in ancient times, peaking around 8 to 11 Gyr ago, corresponding to galaxies observed between $1 < z < 3$.

To link the characteristics of SFHs and galaxy structure —vital for comprehending evolution— spectroscopy is of paramount importance. The amount of information recovered when studying a spectrum is limited by the telescope's spatial resolution. This is because single stars in distant galaxies cannot be resolved and analysed with current observing facilities. Therefore, light from distant objects is treated as an integrated source from unresolved groups of stars (integrated spectrum), and they can be studied by applying spectral synthesis techniques.

Translating observed spectra into physical properties requires (1) isochrones to model all phases of stellar evolution, (2) stellar libraries to calculate measurable fluxes, (3) an Initial Mass Function (IMF) to sample the distribution of stellar masses, and (4) some physical properties of the interstellar medium (ISM) (chemical abundance, dust extinction and dust attenuation, e.g. Conroy 2013). The convolution of these ingredients is known as Stellar Population Synthesis (SPS) technique (Tinsley, 1972; Bruzual et al., 1983; Maraston, 1998; Leitherer et al., 1999; Vazdekis, 1999; Conroy et al., 2009) and is commonly used in Spectral Energy Distribution (SED) fitting codes (Fernandes et al., 2005; Tojeiro et al., 2007; Fritz et al., 2007; da Cunha et al., 2008; Johnson et al., 2021).

While applying SED fitting to integrated spectra enables the recovery of a wide variety of information, this is prone to substantial limitations and uncertainties: stellar population properties estimations suffer from age-dust-metallicity degeneracy (Fritz et al., 2007), and the choice of priors on some characteristics (SPS templates, dust model, IMF, SFH) (Tojeiro et al., 2007; Longhetti & Saracco, 2009; Pforr et al., 2012) can further exacerbate the problem (Fernandes et al., 2005). The innate characteristics of stellar populations impose natural restrictions on our grasp of stellar age, among other parameters (Sawicki et al., 1996). Notably, as stellar populations mature, the distinctions in their optical spectral characteristics diminish.

High spatial resolution spectra are essential for refined outcomes and are obtained from the new generation of instruments, namely Integral Field Unit (IFU) spectrographs. Integral Field Spectroscopy (IFS) boasts several benefits over integrated spectra, including quality spectral resolution and sampling of an entire astronomical object. IFS generates 3D data cubes, offering spatially detailed information for galaxies, improving the capacity to ascertain luminosity-weighted features vital for discerning mixed stellar populations. The adoption of IFS surveys has seen a significant uptick in recent years, spanning nearby and high-z cosmic regions (Bacon et al., 2001; Sánchez et al., 2012; Bundy et al., 2014; Poggianti et al., 2017). However, it is still difficult to objectively assess the fidelity of these methods in recovering the inherent physical properties of galaxies (Fernandes et al., 2013a).

In this context, cosmological hydrodynamical simulations can play a crucial role in studying observational data and exploring and analysing the limitations, biases, and influences from SED fitting recovered parameters (Baes, 2019). The new generation of cosmological simulations, such as EAGLE (Crain et al., 2015), `IllustrisTNG` (Nelson et al., 2018; Pillepich et al., 2018) and the Auriga Project (Grand et al., 2017) –just to name a few–, generate high-resolution galaxy representations. These can be used to simulate the derivation of spatially resolved quantities and draw parallels with intricate observational projects like the Sloan Digital Sky Survey (SDSS, York et al. 2000). Simulations integrating hydro- dynamics and Radiative Transfer (RT) are noteworthy as they can produce simulated observations mimicking real data, for which all physical properties are known.

Employing combined hydrodynamic and RT simulations has served as instrumental tools for comparing SED fitted properties of mock galaxies to actual properties. By examining an isolated disc mock galaxy from varied observational angles, Hayward & Smith (2014) identified variations in derived parameters because of changes to the inclination, the choice of dust attenuation law, and the selection of the IMF. In a separate study, Torrey et al. (2015) used the Illustris Simulation (Nelson et al., 2015) to emulate IFS and detected systematic biases under conditions of constant metallicity and age restrictions for galaxies. Sorba & Sawicki (2015) noted the stellar mass estimates derived from SED fitting are consistently about 25% lower when based on spatially unresolved photometry. An examination of panchromatic SEDs by Goz et al. (2017), revealed significant uncertainties in retrieving stellar mass at both minimal and extensive ranges.

Sophisticated approaches to contrast simulated and actual IFS have been developed. Ibarra-Medel et al. (2019) generated MaNGA-analogous (Bundy et al., 2014) spectra for a duo of Milky Way-resembling simulated galaxies, assessing impacts of elements like inclination, resolution, S/N ratio, and attenuation on the recovered stellar mass and age radial profiles, with considerations for observational challenges such as atmospheric seeing and noise. Discrepancies were noted in discerning stellar populations tied to galaxy spatial configuration and overarching stellar masses. Progressing the narrative, Nanni et al. (2022) introduced IMANGA, an innovative blueprint to spawn mock MaNGA spectral observations, integrating all systemic irregularities detected in the survey data. They generated a data set of 1000 MaNGA synthetic spectra harnessing galaxies from the TNG50 simulation, determining ages, metallicities, and kinematics (Nanni et al., 2023) with 68% confidence level without any systematic bias. In a parallel endeavour utilising the same simulation, Sarmiento et al. (2022) presented MaNGIA, a compilation of mock observations emulating MaNGA survey tools and selection benchmarks, designed to dissect the SFH, age, metallicity, mass, and kinematics of said galaxies. The recovered properties' overall trends were in good agreement with observations.

Not only are stellar population properties affected by degeneracies imposed by different SPS models, but elements like dust attenuation, the S/N ratio and the shape of the SFH also play influential roles (Smith & Hayward, 2018). Research by Carnall et al. (2019) and Leja et al. (2019) demonstrated the impact of SFH priors on SED fitting outputs, revealing variations in stellar mass, SFR, and mass-weighted age estimates. Interestingly, non-parametric SFHs yielded more accurate properties than parametric ones, especially in age and SFR parameters. This assertion was further corroborated by Lower et al. (2020), highlighting the efficiency of non-parametric SFH in RT galaxy simulations from 0.4 to 0.1 dex in SFR and stellar ages. Finally, Qin et al. (2022) examined the degeneracy in SED fitting using local star-forming galaxies and mock spectra with known attenuation parameters. Their analysis revealed a notable degeneration link between SFHs and the attenuation curves with the potential for systematic errors based on the fitting code employed.

The omission of emission lines in SSP templates for spectrum simulations has been a common practice, though acknowledged as a limiting factor. Sánchez et al. (2016) addressed this by incorporating emission lines to their simulated spectra, enhancing the accuracy of determining luminosity-weighted ages and metallicities to approximately ~ 0.2 dex. However, systematic errors emerged due to using different SSP templates and spectral resolutions in SED fitting, and the analysis did not extend to a thorough RT simulation.

Many of the previously discussed studies aim to replicate observational conditions. Still, they lack full RT simulations utilising highly realistic SSP templates—precisely, those featuring ionised gas on younger stellar groups to model star forming regions (Kapoor et al., 2023)-, and considerations of the galaxy's 3D structure, the mix of dust and stars, and viewing angle. These investigations also omit a holistic assessment of all SED fitting priors, including choices related to the IMF, spectral libraries, SFH shape, and dust attenuation law. In this project, we want to explore the reliability and limitations of SED fitting in deriving insights from both observed and simulated galaxies, taking into account stellar and dust geometry, galaxy morphology, inclination, recognised priors like SFH and IMF, and the principles of stellar population synthesis. While studies similar to these have already been performed, our project stands out as it will be the first one of this kind that fully considers the 3D distribution and mix of stars and dust, which will include nebular emission (both continuum and lines) from star formation calculated in a self-consistent and physically motivated manner, and that will be able to simultaneously test the reliability of SFR indicators from UV, emission lines, MIR and FIR. Ultimately, we seek to thoroughly unify these elements to dissect potential discrepancies and systemic errors in SED fitting, as well as push its capabilities to their limits for specific observational characteristics. Table 1 presents comparative insights with other research.

Understanding galaxies through spectral synthesis has challenges, biases, and uncertainties. While many studies have set the stage, a comprehensive exploration using spectral synthesis on simulated data stands out as a paramount approach to untangling these intricacies. In this research, we intend to harness this tool, providing a comprehensive analysis that bridges existing knowledge gaps and further advances our understanding of galaxy evolution.

Component	This project	Ibarra-Medel et al. 2019	Nanni et al. 2022	Sarmiento et al. 2022
Simulations	TNG50 Nelson et al. (2018) Pillepich et al. (2018)	ART Kravtsov et al. (1997)	TNG50 Nelson et al. (2018) Pillepich et al. (2018)	TNG50 Nelson et al. (2018) Pillepich et al. (2018)
RT code	`SKIRT` Baes et al. (2011) Baes & Camps (2015)	×	`SKIRT`[a] Baes et al. (2011) Baes & Camps (2015)	×
SSP templates	FSPS Conroy et al. (2009) Byler et al. (2017)	GSD156 Fernandes et al. (2013b)	MaStar Maraston et al. (2020)	MaStar-sLog Sánchez et al. (2022)
SED fitting code	`SINOPSIS` Fritz et al. (2007) Fritz et al. (2011)	Pipe3D Sánchez et al. (2016)	Firefly Wilkinson et al. (2017)	pyPipe3D Lacerda et al. (2022)
Emission lines in spectra	✓	✓	✓	×
Number of mocks	~ 2500	8	2	10000
Testing SFR indicators	✓	×	×	×

[a] not full simulations.

Table 1: Comparison with similar works.

2 Hypothesis and Objectives

While numerous studies exist in the literature on deriving properties of galaxies from spectra, the nature of the biases to which the derived physical properties are subject needs to be further studied, with models as physically motivated as possible.

In our study, we rest on two pivotal assumptions: firstly, that hydrodynamical simulations aptly mirror the physical characteristics of the stellar populations in galaxies across cosmic time encompassing age, metallicity, and spatial distribution (i.e. morphology). Secondly, that SPS accurately describes the star properties in galaxies, facilitating the extraction of their physical properties. Hydrodynamical cosmological simulations, rooted in the ΛCDM framework, have been shown to yield simulated galaxy properties which are very close to the observed ones (Guedes et al., 2011; Crain et al., 2015; Pillepich et al., 2018), and SPS remains a preeminent tool for understanding stellar populations properties (Fritz et al., 2011; Ibarra-Medel et al., 2019; Leja et al., 2019).

Our research targets these key questions:

1. What systematic biases arise in the recovery of the stellar population properties using both integrated and integral field spectra?
2. Are results influenced by factors like the galaxy orientation, morphology, physical resolution or dust properties?
3. What is the trustworthy threshold for the SFH resolution (in terms of age bins)?
4. How impactful is the IMF, and how do assumptions on this bias the results?
5. How do selected dust properties affect the SFH recovery, especially the recent SFR?
6. How accurate are recent SFR indicators like UV and Hα luminosity and MIR and FIR emissions? What is the relative amount of optically visible and invisible SF as a function of other galactic properties?

We are committed to dissecting the trustworthiness, limits, biases, and potentialities of stellar population synthesis techniques applied to simulated observations of galaxies, covering both global and spatially resolved spectra. Additional goals include:

- Generating a collection of synthetic spectra observations of galaxies for diverse morphologies
- Contrasting the biases seen when employing integrated and integral field spectra for each galaxy
- Investigate how data resolution in SED fitting influences outcomes
- Evaluate results by controlling physical characteristics: morphological type, geometry, adopted IMF and/or SFH, and mimicking different instruments such as MUSE spectrograph.

3 Methodology

3.1 Illustris TNG50 simulation

The `IllustrisTNG`[1] (Pillepich et al., 2018; Nelson et al., 2018; Springel et al., 2018; Marinacci et al., 2018) project is the latest state-of-the-art cosmological magnetohydrodynamical simulation, based on the moving-mesh code Arepo (Springel, 2010), solving hydrodynamic equations on an adaptive moving Voronoi tessellation. The cosmology adopted is ΛCDM Planck data: $\Omega_m = 0.3089$, $\Omega_b = 0.0486$, $\Omega_\Lambda = 0.6911$ and $h = 0.6774$ (Adam et al., 2016).

The simulation suite encloses three simulation scales: `TNG300`, `TNG100` and `TNG50`. We have opted to use `TNG50` for this study due to its finest resolution within `IllustrisTNG` with a $(50Mpc)^3$ comoving volume and mass resolution of $m_b = 8.5 \times 10^4 M_\odot$. Following the approach of Trčka et al. (2022), we selected galaxies at $z = 0$ with stellar mass inside twice the stellar half mass radius of at least $10^8 M_\odot$ for adequate particle representation. This criterion provides us with a collection of roughly 2500 galaxies.

3.1.1 Subsample selection

A subset of 10 galaxies from the primary sample has been handpicked for the first phase of the project. Table 2 lists the core attributes of these selected galaxies. We have opted for diverse morphological types, resulting in a diverse set of total stellar mass, SFR, and metallicity. Milky Way (MW) like galaxies were taken from Pillepich et al. (2023) and Emami et al. (2021), and the rest are from Zana et al. (2022) and Engler et al. (2021). Figure 1 illustrates eight of the ten galaxies from the subsample.

Subhalo ID	Type	Total$_*$ Mass [$10^{10} M_\odot$]	Age (Gyr)	SFR [$M_\odot yr^{-1}$]	Z_{gas}
3	Elliptical	9.25	10.0	0	0.037
338447	Spheroidal	6.31	11.4	0	0.020
372755	MW like	6.91	5.63	11.9	0.012
388544	MW like	18.4	6.78	8.10	0.008
392277	MW like	5.14	8.36	0.930	0.008
402555	MW like	13.7	7.66	1.73	0.009
427211	MW like	14.5	6.42	1.36	0.009
429471	Elliptical	12.8	10.1	0.0003	0.700
519311	Spiral	9.23	6.92	2.50	0.013
630870	Disk	1.26	6.77	0.45	0.006

Table 2: Primary characteristics of the galaxy subsample. Data extracted from the hydrodynamical simulation was cleaned to remove superfluous values, resulting in an average of the remaining data. The age was calculated as the subtraction between the age of the universe and the exact time (given as the scale factor) when each star was formed.

3.2 Post-processing with `SKIRT`

`SKIRT`[2] (Stellar Kinematics Including Radiative Transfer) (Baes et al., 2011; Camps & Baes, 2015, 2020) is a state-of-the-art code performing 3D continuum radiative transfer in astrophysical systems to simulate the interaction between dust and radiation employing Monte Carlo (MC) method. Using the MC technique, `SKIRT` treats the radiation field as photon packages, which are followed through the dusty system, taking different trajectories simulating emission, absorption and scattering events. This code also allows a variety of complex geometries and snapshots from hydrodynamical simulations to simulate Active Galactic Nuclei (AGN) activity (Stalevski et al., 2012; Stalevski et al., 2019), molecular clouds (Monceau-Baroux & Keppens, 2017; Jáquez-Domínguez et al., 2023), mock galaxy photometry and spectroscopy (Saftly et al., 2015; Trayford et al., 2017; Kapoor et al., 2021; Trčka et al., 2022), among others.

[1] https://www.tng-project.org/
[2] https://skirt.ugent.be/

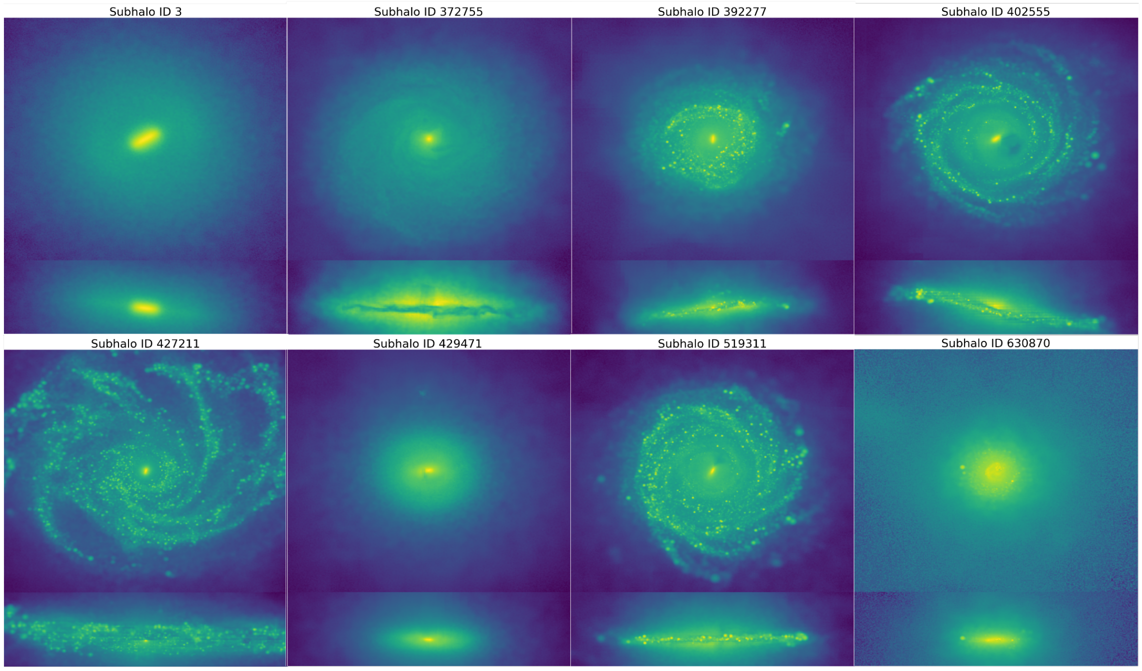

Figure 1: Face-on and edge-on synthetic V band images cutouts of the galaxy subsample at $z = 0$ for this study.

3.2.1 Input model from hydrodynamical snapshots

In this work, we are applying `SKIRT` to the `Illustris TNG50` simulation to mimic real galaxy observations. We partly follow the methodology from Kapoor et al. (2021) and Trčka et al. (2022), as illustrated in fig. 2 with some variations:

Evolved stellar particles. All information about these particles comes from the hydrodynamical simulation. Particles with ages above 10 Myr are considered evolved stars, and we assign a SED from the Flexible Stellar Population Synthesis (FSPS, Conroy et al., 2009) libraries (neglecting nebular emission and assuming a Kroupa 2002 IMF) depending on the age, metallicity and mass.

Star-forming regions. The remaining star particles, younger than 10 Myr and not classified as stellar wind particles, are considered SF regions. We are assigning a SED from FSPS containing nebular emission (Byler et al., 2017) along with an IMF of choice for a young star particle. Each SF particle is characterised by metallicity, birth mass, age and ionisation parameter ($log(U)$). For the early stages of the investigation, we are setting $log(U) = -2$ as in Vogelsberger et al. (2020) and Nagaraj et al. (2022). Nevertheless, in future plans, we are studying the variations when changing $log(U)$ as different ionisation parameters are observed in real environments.

Dust cells. This component is used to derive the geometrical distribution of interstellar dust as `Illustris TNG50` simulation does not include dust physics. Eligible gas cells are selected by the criteria of Torrey et al. (2012) that separates the hot circumgalactic medium from the cooler gas. For each selected cell, the dust density is $\rho_{dust} = f_{dust} Z_{gas} \rho_{gas}$, where Z_{gas} and ρ_{gas} are the metallicity and density gas, respectively, and come directly from the hydrodynamical simulation. f_{dust} is a fixed parameter varying between $0.2 < f_{dust} < 0.7$ (Saftly et al., 2015), and it represents the amount of metallic gas contained in dust grains. The assumed dust model is The Heterogeneous dust Evolution Model for Interstellar Solids (`THEMIS`) by Jones et al. (2017) as it is laboratory-based and has undergone extensive evaluation in the context of the DustPEDIA project (Davies et al., 2017).

Other parameters. The geometrical distribution of dust is discretised in RT simulations, and to represent the dust grid at best, we are using an octree grid with a maximum cell dust fraction of 10^{-6}. A number of 10^{10} photon packets are being deployed to achieve a reasonable S/N, resembling the MUSE GASP data (Poggianti et al., 2017), and to reduce the Monte Carlo noise. Our galaxy sample is observed from different viewing angles, including face-on, edge-on, and 45 to 70 degrees.

Instruments. Two formats of output are being set up: integrated and spatially resolved spectra. For each type of file, we aim to mimic MUSE observations with characteristics as follows: (1) a linear grid of 3682 points on the wavelength rage of $4700 < \lambda(\text{Å}) < 9300$, (2) a field of view of 1×1 $arcmin^2$, and (3) a spatial sampling of 0.2×0.2 $arcsec^2$.

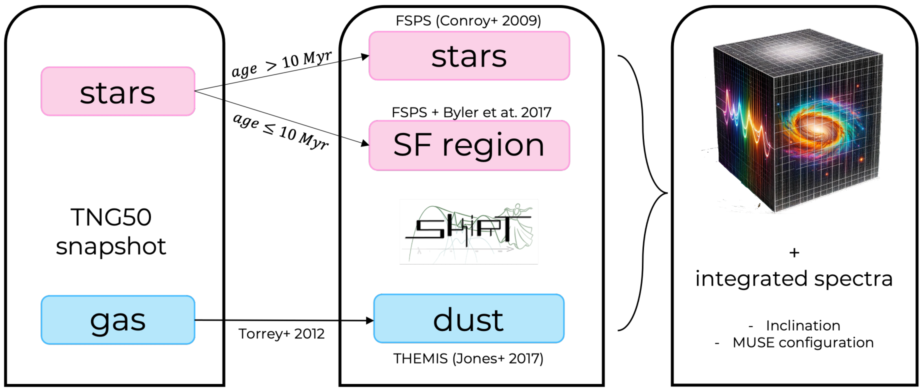

Figure 2: Graphic overview of the radiative transfer simulation. The data cube image was generated with DALL · E on 16/11/23.

3.2.2 FSPS into SKIRT

Galaxy components are characterised by different SEDs, e.g. stars emit as continuum radiation, and HII regions contain massive stars that account for nebular lines and continuum free-free emission. To reproduce galaxy observations in the best possible way, we need to include these effects on SSP templates.

Over the last couple of years, SKIRT users have devoted a great deal of effort to reproducing real galaxy observations from cosmological simulations. One of the main features is that SKIRT can account for continuum or line SEDs when doing the simulation. Nevertheless, real observations show a combination of continuum and nebular emission. As SKIRT does not correctly combine these two emissions, we are implementing the FSPS library with nebular emission lines to have the continuum and lines' luminosity appropriately calculated when the MC technique is applied. To accomplish this, FSPS templates are modified to attain a certain wavelength sampling for SKIRT to work correctly on this frame.

3.3 Spectral Synthesis Code

SINOPSIS, abbreviated as SImulatiNg OPtical Spectra wIth Stellar populations models[3] (Fritz et al., 2007, 2011, 2017) is a spectrophotometric code based on the stellar population synthesis technique that searchers for the best model spectra reproducing the equivalent widths (EW) of the main absorption and emission lines and predefined continuum bands of observed spectra. SINOPSIS tries to minimise a χ^2 function, which assesses the likelihood between the observed and model spectrum by using an adaptive simulated annealing algorithm. The model spectrum is created by summing up synthetic spectra from SSPs of various ages. Each SSP is subjected to extinction to replicate the presence of a uniformly distributed dust screen in front of the stars. The resulting synthetic spectrum denoted as $F_{mod}(\lambda)$ (model flux)is formulated as:

$$F_{mod}(\lambda) = \sum_{i=1}^{N_{SSP}} M_i \cdot L_i(\lambda) \cdot 10^{-0.4A(\lambda)R_V E(B-V)_i}, \tag{1}$$

where N_{SSP} is the number of SSP used and M_i and $L_i(\lambda)$ denote the stellar mass and the luminosity spectrum for the $i-th$ SSP. The extinction component is accounted for by the extinction law $A(\lambda)$, normalised to the V band, and the value of R_V, varying with the extinction curve. The fitting involves two free parameters: the colour excess $E(B-V)_i$, dictating extinction based on age, and the stellar mass or SFR for each SSP age. This model incorporates selective extinction, indicating higher dust extinction for younger stellar populations, which are typically located in dustier zones where they were born. The SINOPSIS code is based on the premise that all stellar

[3] https://www.irya.unam.mx/gente/j.fritz/JFhp/SINOPSIS.html

populations in a galaxy maintain a consistent metallicity value across various ages. The code then evaluates the observed spectrum, adjusted for Milky Way extinction, against a range of synthetic spectra. This process seeks to find the ideal combination of mass and extinction values that accurately replicate the observed spectrum, with the best fit being determined by minimising a specific goodness function Γ as in:

$$\Gamma = \sum_{j=1}^{N} \Gamma^j = \sum_{j=1}^{N} \left(\frac{F_o^j - F_m^j}{\sigma^j} \right)^2 , \tag{2}$$

having F_o^j and F_m^j as the average fluxes (or EW) calculated over the jth band of the observed and model spectrum, respectively. σ^j is the uncertainty on the observed flux (EW) in that band. The main features of this code are that there are no predetermined models as it searches for the best combination of parameters and that non-parametric SFH allows a very flexible treatment of dust extinction.

Broadly speaking of the adjustment, each of the different SSP spectra is scaled by its age-specific SFR value, with the algorithm endeavouring to reduce a χ^2 function, aiming to find the ideal SFR mix to match the actual spectrum. As seen in Fritz et al. (2007), key emission and absorption lines are also used for comparison. An adjustable simulated annealing technique navigates the parameter domain, targeting the χ^2 function's lowest point. The combination of parameters that best fit the observed spectrum is a nonlinear problem but also lacks sufficient constraints for its parameters. Due to factors like limited wavelength analysis and age-metallicity interplay, the outcome is degenerated. To bolster the trust in the findings, `SINOPSIS` runs 11 optimisation iterations and chooses a median mass model, assigning error rates to elements based on different algorithmic starting points.

`SINOPSIS`, as default, uses the latest models of S. Charlot and G. Bruzual (CB23, 2023 in prep.), containing emission lines for SSPs with ages $< 20Myr$, calculated with `Cloudy` code (Ferland et al., 2017). CB23 spectra are composed of 220 ages that are re-binned into 12 main age bins ranging from 10^4 to an adjustable upper age limit, expressed either in terms of a specific age or redshift, based on a cosmology with $H_0 = 70$, $\Omega_\Lambda = 0.70$, and $\Omega_M = 0.30$. Due to degeneracies, these 12 bins are further re-binned into four for the calculation of the final SFH as seen in table 3. In addition, `SINOPSIS` can also use FSPS, Bruzual & Charlot (2003) and Jacoby (Jacoby et al., 1984) models as well.

$SFR_i bin$	Lower Age	Upper Age
SFR_1	0	19.6 Myr
SFR_2	19.6	571 Myr
SFR_3	571 Myr	5.75 Gyr
SFR_4	5.75 Gyr	14 Gyr

Table 3: Time spans used by `SINOPSIS` to derive the SFH.

To recover the observed spectrum, the code utilises a Kroupa (2002) IMF with stellar masses from $M_* = 0.1$ to $150M_\odot$ with metallicity values from $log(Z/Z_\odot) = -2.5$ to $log(Z/Z_\odot) = 0.5$ with $Z_\odot = 0.014$. By opting for a single final Z value throughout all age bins of the SSPs, `SINOPSIS` limits the number of fitted parameters by picking the value that most accurately mirrors the data. The integrity of this procedure has been tested in Fritz et al. (2007) through analysis of synthetic spectra with differing SFHs and metallicity dependent on stellar ages (mimicking galaxy chemical changes). The findings reveal that the treatment of metallicity does not introduce substantial bias into the determined stellar mass or SFH.

Using a spectrophotometric code helps infer attributes such as total stellar mass, SFR across cosmic time, extinction, and a sole 'brightness-weighted' metallicity of the stars laying in galaxies whose radiance forms are reflected in an integrated spectrum or spatially resolved spectra.

Given that `SINOPSIS` does not employ a wavelength-by-wavelength comparison approach between model and observed data, but rather relies on the assessment of average flux within specific spectral bands, the precise selection of these bands carries significant importance. For the sake of our investigation, several tests were conducted to establish the final continuum bands for use in `SINOPSIS`. The starting point was the predefined bands of the code (Fritz et al., 2017), followed by the bands from Moretti et al. (in prep.), and finally, the two sets of bands proposed in this work. We observed lower χ^2 values when Moretti et al. bands were used. Nevertheless, the new set of bands offered a better spectral shape as they span the entire MUSE wavelength range. Based on these findings, we opted for broader continuum bands due to their advantageous lower χ^2 values and minimised error in parameter recovery.

The core objective of this Thesis is to evaluate the precision of the retrieved SFH and investigate the limits of age resolution. For this purpose, we implemented a k-means algorithm to classify the ages of the SSPs into a series of bins. This will enable us to determine the optimal number of SSPs of varying ages for the fitting process, aiming to maximise the likelihood of obtaining the most realistic SFH. Factors taken into consideration included the equivalent widths of nine distinct emission and absorption lines, as well as the D4000 indicator and the $B-V$ colour excess. Figure 3 demonstrates that the combination of the elbow method with the silhouette score recommended $k=19$ as the optimal number of clusters (bins). However, we plan to further investigate the potential of using $k=25$ to explore whether this increased number of time bins can further refine the recovered SFH resolution.

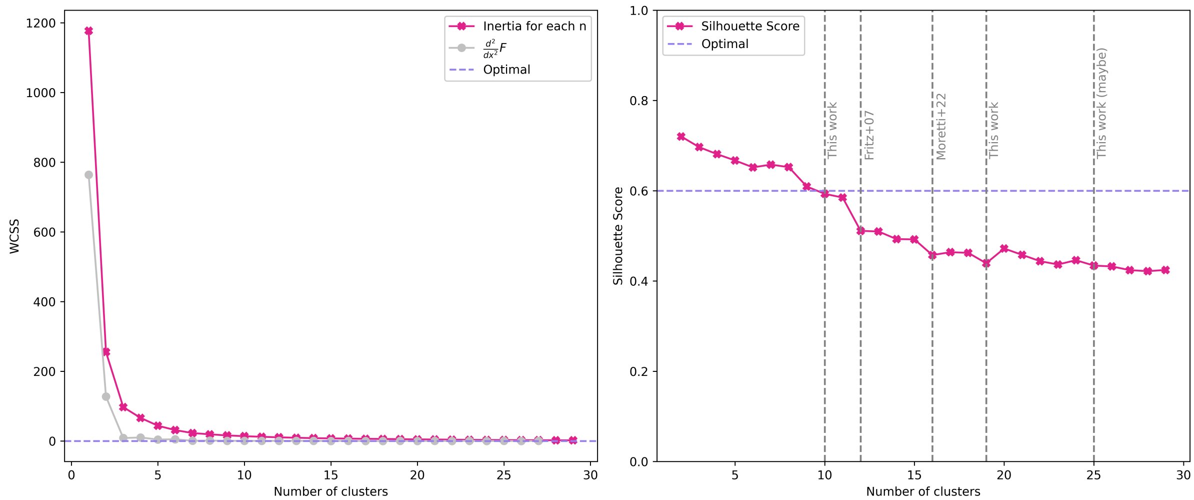

Figure 3: k-means algorithm results. The left panel displays the Within-Cluster Sum of Squares (WCSS), illustrating the sum of squared distances between each point and its cluster's centroid, with the WCSS being highest at $k=1$. The right panel shows the silhouette score ranging from -1 to 1, where a score of 1 means distinct clusters, 0 indicates clusters are intermingling, and -1 implies potential misplacement of samples in clusters.

Similar to figure 1 in Fritz et al. (2007), figure 4 displays our results for the 19-time bins from the FSPS templates. At the youngest and oldest ages, the binning aligns closely with `SINOPSIS`'s default. The most prominent variation is seen from roughly 3 to 100 Myr, where the time bins are more narrowly set. Continuity between adjacent SSPs was meticulously maintained. While the EW in Jacoby libraries for younger ages spans 5 to 1000 Å, it ranges from 50 to 300 Å in FSPS libraries. Table 4 outlines the ages and associated time intervals Δt, indicating periods where we consider the SFR in a given population to be constant. We aim to conduct a similar analysis with the latest CB23 libraries.

Age interval [yr]	Δt [yr]	Age interval [yr]	Δt [yr]	Age interval [yr]	Δt [yr]
0 - 1×10^5	1×10^5	6.3 - 7.9×10^6	1.6×10^6	6.3×10^8 - 1×10^9	3.7×10^8
1 - 1.8×10^5	0.8×10^5	7.9×10^6 - 1×10^7	2.1×10^6	1 - 2.5×10^9	1.5×10^9
1.8×10^5 - 4×10^6	3.82×10^6	1 - 1.6×10^7	0.6×10^7	2.5 - 4.5×10^9	2×10^9
4 - 4.5×10^6	0.5×10^6	1.6 - 4×10^7	2.4×10^7	4.5- 9×10^9	4.5×10^9
4.5 - 5×10^6	0.5×10^6	4×10^7 - 1.1×10^8	7×10^7	9 - 14×10^9	5×10^9
5 - 5.6×10^6	0.6×10^6	1.1 - 4.5×10^8	3.4×10^8		
5.6 - 6.3×10^6	0.7×10^6	4.5 - 6.3×10^8	1.8×10^8		

Table 4: Ages and duration for the 19 bins of the averaged SSP spectra from the machine learning algorithm.

Constrained EW for the fit are documented in Table 2 in Fritz et al. (2007). Given that the MUSE wavelength range only accounts for five of the fourteen lines, we contemplate extending the analysis to include lines beyond $H\alpha$. However, the resolution of the FSPS libraries diminishes past this range, suggesting the possibility of utilising alternative spectral libraries for these additions.

We ultimately opted for two variations of the extinction law: firstly, the Milky Way version from Cardelli et al. (1989), and secondly, the Calzetti law from Calzetti et al. (1994).

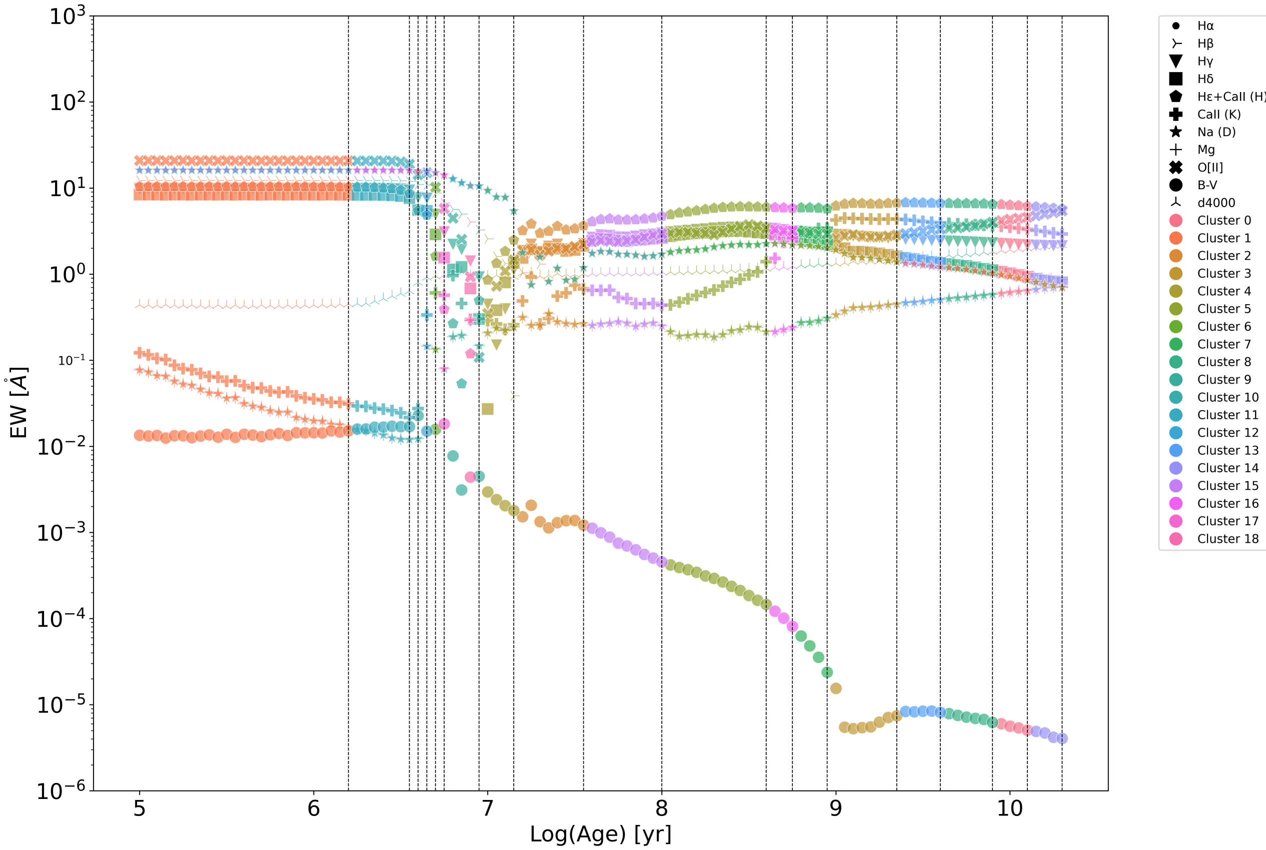

Figure 4: Equivalent width values of lines, $B - V$ colour excess and the D4000 index across the full range of SSP spectra. We present the absolute values of EW in Å for clarity. Vertical dashed lines demarcate the time intervals of the 19 averaged SSPs, in accordance with table 4.

4 Results

We then examine the characteristics derived from the integrated spectra of a subset of galaxies. This is to assess any variances in the recovered parameters, in an effort to identify possible biases and limitations. This evaluation relies on results from the `SINOPSIS` SED fitting code and data from the `SKIRT` radiative transfer code, integrated with the `IllustrisTNG` hydrodynamical simulation. It is important to note that we used FSPS to fit FSPS-produced spectra to maintain the most straightforward comparison.

4.1 Fitting spectra

In figure 5, the integrated spectra and their corresponding best fit models for Subhalo ID 3 at $i = 0°$ are shown, using three different combinations of extinction laws and time binning. Regions used for continuum band flux calculations are highlighted in grey. Each model yielded a notably low χ^2, particularly the one that combines the Calzetti law with the newest binning approach. The bottom panel illustrates the residual values for each model across the wavelength range. The residuals for the left and right models centre around zero, whereas the middle model shows a peak residual near 0.05 (5%). We note that all models closely match the observed data, accurately capturing the overall shape of the spectra. This trend is followed by all the early-type galaxies in our sub sample.

The fitting accuracy for late-type galaxies, in contrast, does not reach the level seen in early-type galaxies. This is evident in fig. 6 for Subhalo ID 519311, where an overestimation of some emission lines is observed, most notably ionised oxygen doublet [OIII] lines at $\lambda = 4959$Å and $\lambda = 5007$Å. Despite not being constrained in our model and conducting various tests to better fit the [OIII] lines, the results remained unchanged. Contrary to expectations that the optimal fit would occur at $i = 0°$ due to the distribution of dust and stars across the galaxy, the most accurate fit was found at $i = 70°$.

Another noteworthy aspect to consider is the χ^2 values, which are minimized and perform at their best, even

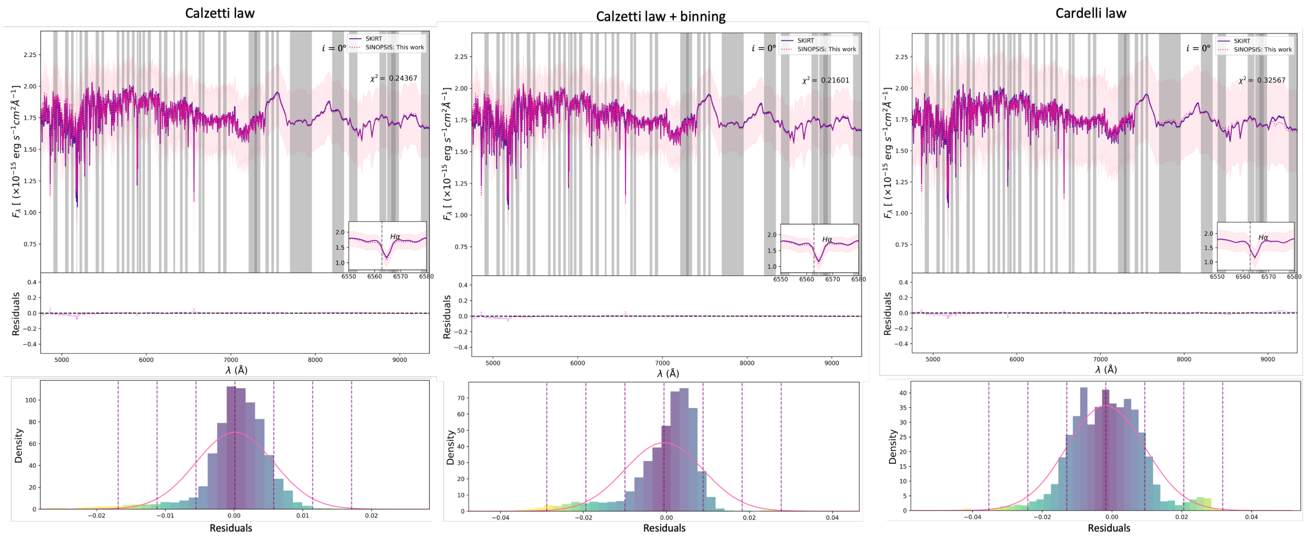

Figure 5: Best fitting models (indicated by dotted pink lines) for Subhalo ID 3 (purple), applying three variations of extinction laws from the `SINOPSIS` SED fitting code. The smaller subpanels below display the residuals for each wavelength, comparing the best fit to the actual observed spectrum.

though we have not considered [OIII] in the calculations. The best fit at $i = 70°$ exhibits a smoother residual distribution compared to the uneven ones in the other fits. An adjustment in extinction values might lead to an improvement in the fit, potentially resulting in a reasonable χ^2 as reported in Villa-Vélez et al. (2021).

4.2 Mass

Fitting the principal features of an integrated optical spectrum enables the assessment of various properties of stellar populations, including the total stellar mass. `SINOPSIS` provides three distinct estimates of stellar mass as described by Longhetti & Saracco (2009). We selected the second approach, which includes the mass of stars still in the nuclear burning stage and remnants (such as white dwarfs, neutron stars, and black holes), excluding the mass lost through stellar evolution and supernova events.

While the spectral shape fits were comparably accurate, when run on the integrated, MUSE-like spectra, `SINOPSIS` consistently yielded lower mass estimations with respect to the real values. The relative error deviation, calculated as $F_{SKIRT} - F_{SINOPSIS}/F_{SKIRT}$, from the three SED fitting methods, as seen in fig. 7, were alike, predominantly peaking between 9 and 15. The error margins, as suggested by the similarities in mean error and standard deviation under both the Cardelli and Calzetti laws with the new bin setup, are reduced to around 10%. However, discrepancies between actual and fitted data are likely to increase. A systematic underestimation in mass recovery is evident though the consistent use of FSPS templates in both RT simulations and SED fitting. The largest discrepancies are observed in late-type galaxies with steep inclinations as that the presence of dust can greatly impact the mass estimate (Sorba & Sawicki, 2015).

4.3 Star Formation History

Figure 8 and 9 show representative examples of the recovered SFHs of the forty galaxies. For early-type galaxies, good fits to the observed data are achieved using the Calzetti law with the binning proposed in this project, closely mirroring the overall SFH shape. Another important observation in fig. 8 is that the Cardelli law yielded the best-fit results. It is now essential to investigate this law with the new binning scheme to assess potential enhancements in the results.

Despite observing slight variations in the SFH profiles of elliptical galaxies, the spectra remain consistently similar at all inclinations, which serves as a positive indicator for RT simulations and the SED fitting code. The real SFHs of a galaxy, depicted by dotted lines in fig. 8, are influenced by the use of varied time-binning methods. It is crucial to recognise that the chosen binning for the SFH may introduce biases, and enhancing the resolution, perhaps by using 19 time bins instead of the standard 12 used by `SINOPSIS`, might allow for a more accurate SFH

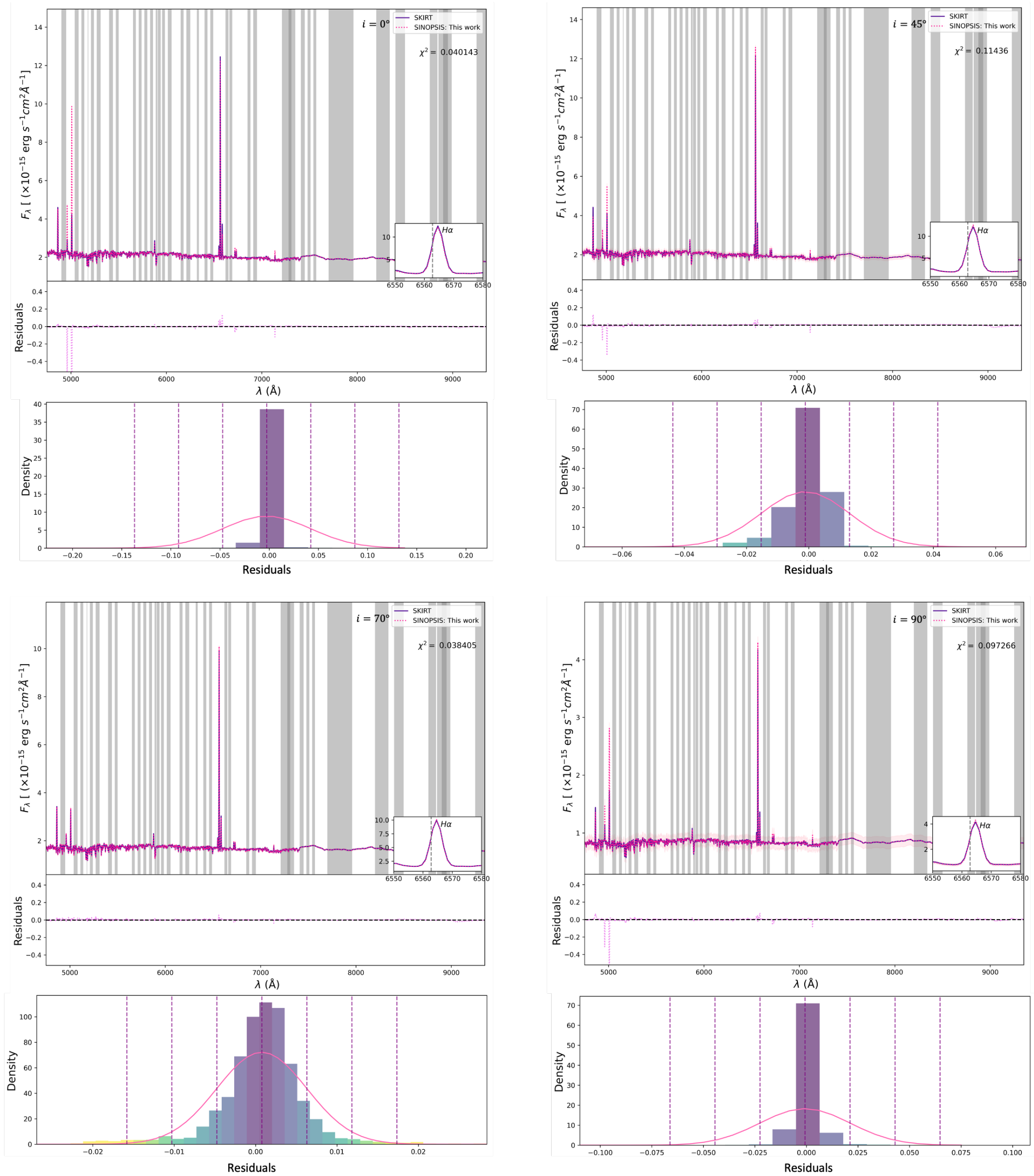

Figure 6: The best fit models for Subhalo ID 519311 at various inclinations, according to the Calzetti law with the most recent binning approach. The spectral shapes, in general, do not exhibit a consistent agreement with the spectra of all galaxies.

modelling. Nevertheless, we are aware that the calculation of the SFH at the youngest ages of the universe increases the uncertainty, as demonstrated in e.g. Johnson et al. (2021).

The fitted SFH for late-type galaxies display a pattern similar to their actual SFHs, although deviations are more pronounced at younger ages. This difference is particularly evident in the final two age bins, with a variation of approximately 10 $M_{\odot} yr^{-1}$. The SFH patterns become more disordered with increased inclinations, particularly at $i = 90°$.

Furthermore, upon comparing figures 8 and 9, it might be worth considering the introduction of a prior for morphological galaxy classification, to explore whether SFH calculations should vary depending on the galaxy type and associated time binning configuration.

As shown in Hayward & Smith (2014) and Smith & Hayward (2018), our findings reaffirm that different viewing angles impact the perceived star formation history, influenced by factors such as dust obscuration and the geometry of star-forming regions. The significant discrepancy observed at $i = 90°$ points to the considerable effect of the subhalo's structure on the mock observations, where dust extinction becomes more critical as the viewing angle

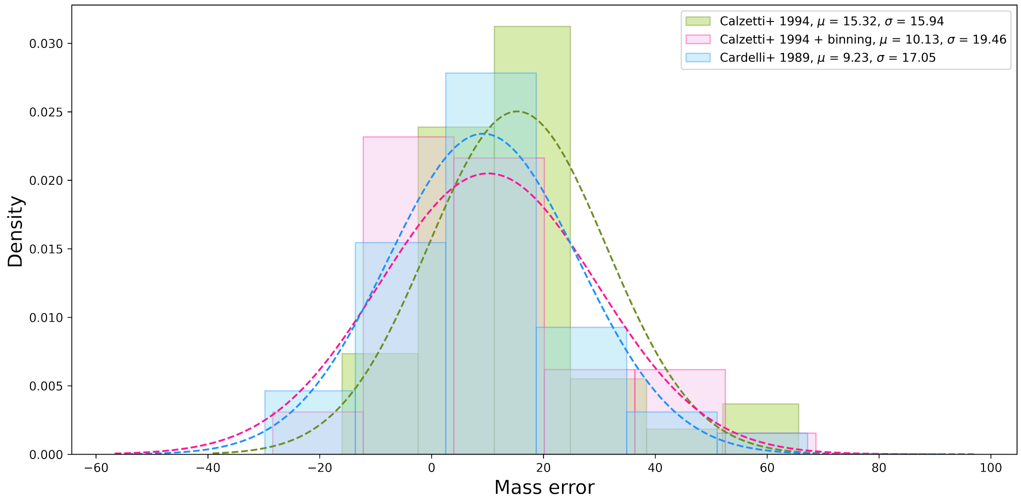

Figure 7: Deviations for the recovered masses in comparison to real values.

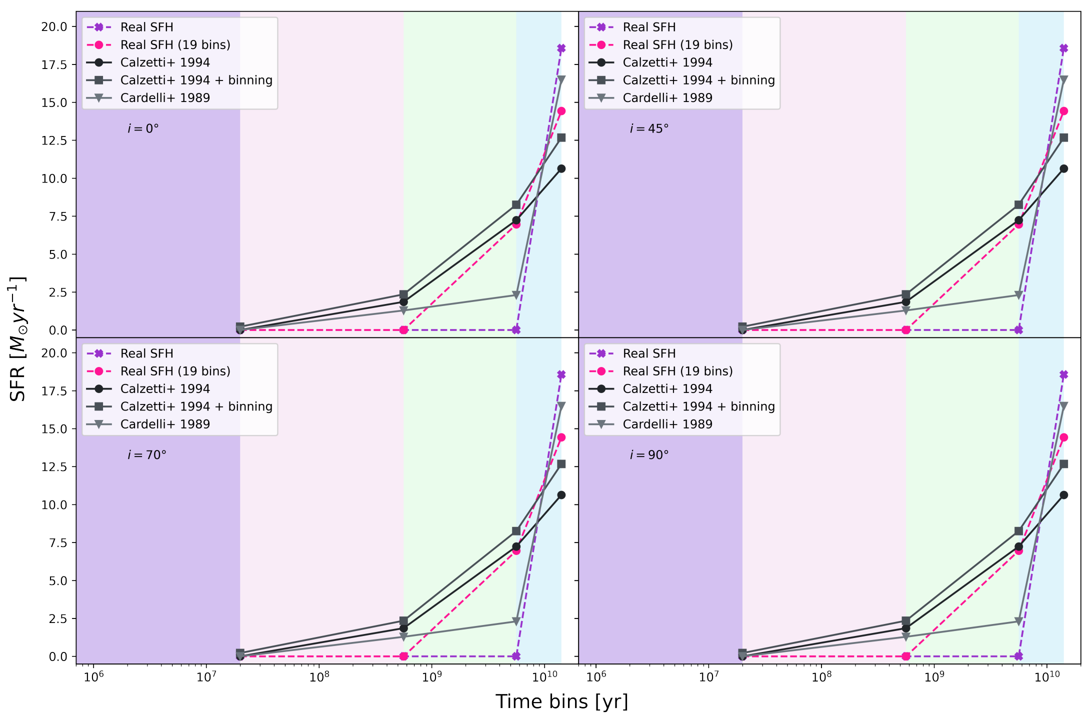

Figure 8: Four panels showing the SFH of an elliptical galaxy (ID 3) from different observational angles. The dotted lines indicate the actual SFH, varied by time binning, while the other lines show the fits obtained from the `SINOPSIS` SED fitting code.

increases. Additionally, it should be taken into account that the method for calculating the age bins for SFH may need to vary for different galaxy types, considering factors such as spectral resolution and other aspects, as outlined in Tojeiro et al. (2007).

For a more accurate estimation of the SFH, it is essential to analyse additional spectral features beyond the MUSE wavelength range. Looking ahead, we plan to broaden our research to cover the UV segments of the spectra,

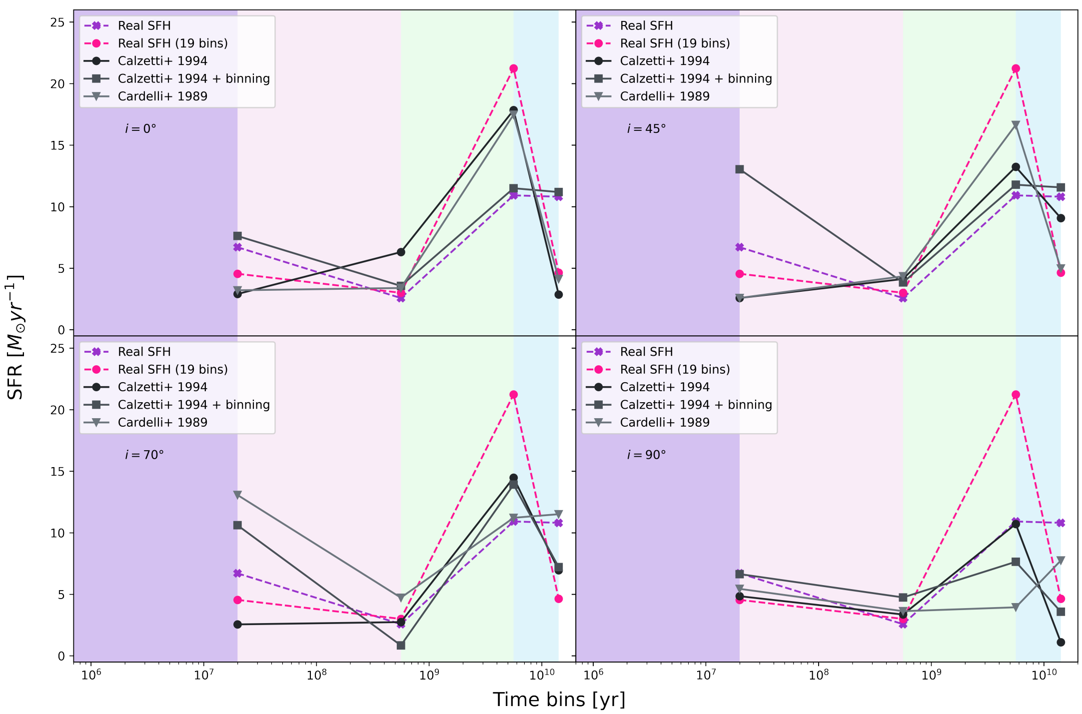

Figure 9: SFH of a spiral galaxy (ID 519311) following the same logic as in fig. 8.

which will be facilitated by the soon-to-be-launched Blue MUSE (Richard, 2019).

4.4 Discussion

In this report, I have presented initial steps and outcomes from a systematic exploration of the potential and constraints associated with applying stellar population synthesis techniques to derive the physical properties of galaxies, with a specific focus on star formation history based on their observed optical spectra. To establish a robust foundation for this study, I first optimised radiative transfer simulations for simulated galaxies and then concentrated on defining fundamental characteristics of the stellar populations that exert a noticeable influence on SFH recovery. These characteristics include the age bins used to define both the spectral fitting's SSP model and the bins used to compute SFH from the fitting results. I began by constructing integrated spectra for galaxies with varying morphologies as if they were derived from summing all the spectra acquired by the IFU spectrograph MUSE at the VLT. Despite the absence of spectral information below $\sim$ 4600 Å, which contains crucial stellar age indicators, SFH reconstruction was successful for the two elliptical galaxies in the sample. While there was an overrepresentation of young stellar populations compared to the "ground truth" (the SFH directly from simulations), it is noteworthy that this outcome was surprisingly satisfactory, considering the use of integrated spectra and less-than-optimal spectral coverage. When analysing galaxies with later-type morphologies, the results understandably showed lower accuracy due to their more complex SFH, leading to a diverse mix of stellar populations. Nevertheless, the overall SFH patterns remained discernible.

A further point of concern is the effect of employing diverse priors for the SFHs, as these may contribute to the disparities seen in the SFHs deduced by the SED fitting code. We aim to assess how these distinct priors alter the shape of the SFH and affect the parameters recovered. Jain et al. (2023) observes that adopting a non-parametric approach to SFH enhances the accuracy of inferred stellar masses, ages, and specific star formation rates (sSFR), a finding consistent with previous research (Leja et al., 2019; Carnall et al., 2019). Despite this, our research is exploring various SFH priors beyond just the non-parametric method.

Moreover, the approach to dust treatment, the selection of spectral libraries, and the choice of IMF are critical factors that can significantly alter the results. In line with Qin et al. (2022), our exploration of different extinction laws within SINOPSIS has revealed that this choice can affect the extent of mass and SFH underestimation. By applying the same FSPS templates in both RT simulations and SED fitting, our results provide support for the conclusions drawn by Sánchez et al. (2016). They emphasise that utilising diverse SSP templates can lead to variations in the recovery of galaxy properties and underline the importance of maintaining template consistency to prevent systematic parameter retrieval errors arising from differences in spectral resolution and parameter space exploration.

This investigation will extend beyond integrated spectra to include spatially resolved spectra as well.

5 Summary and future work

We present measurements of masses and SFHs of global spectra for ten galaxies at four different inclinations to better understand the systematics in galaxy property estimates. The fitting of the integrated spectra was performed using a free-free SFH model, with three different treatments of the extinction law: (1) Cardelli's Milky Way model, (2) the original Calzetti law, and (3) an adapted version of the Calzetti law with new time binning.

Key findings to date include:

- Adding more continuum bands to SINOPSIS effectively minimises χ^2 values.
- The use of machine learning for categorisation aids in refining the time binning associated with SFH, resulting in better SFH resolution.
- While early-type galaxies align well with the best fit model in spectral shape, late-type galaxies display variances in certain emission lines crucial for determining SFR over time.
- Mass estimations across the three SINOPSIS setups display comparable trends and error variances, with the Calzetti law using the new time binning method being the most precise.
- Alterations in time binning when calculating SFH result in varied SFH patterns for the same galaxy, indicating the sensitivity of SFH shape to time binning.
- For a more accurate determination of galaxy properties in relation to SFH, a thorough analysis beyond the MUSE wavelength spectrum is necessary.

The upcoming phases of our study will focus on:

- Further refining the 19 time bins to adjust extinction values and curves, creating distinct setups for steep inclinations.
- Applying our analytical methods to spatially resolved spectra.
- Experimenting with different SFH models, like the tau model, and incorporating varied spectral libraries into the fitting process.
- Broadening the range of RT simulations to assess star formation indicators like UV and $H\alpha$ luminosity.

The work completed during the first three semesters is visually summarised in figure 10.

This work presents an analysis of the masses and SFHs from the global spectra of ten galaxies at four inclinations to understand the systematics in galaxy property estimation. Key findings include the effective minimisation of χ^2 values through additional continuum bands in SINOPSIS, improved SFH resolution via machine learning-enhanced time binning, and noticeable spectral shape similarities in early-type galaxies compared to late-type galaxies. The study concludes that further research beyond the MUSE wavelength spectrum is vital to effectively constrain galaxy properties associated with SFH, such as the D4000 value and the $CaII$ triplet, among others.

Figure 10: This Gantt chart illustrates the timeline for the PhD project, which has followed the original plan without deviation.

References

Adam R., et al., 2016, *Planck 2015 results-I. Overview of products and scientific results*, Astronomy & Astrophysics, 594, A1

Allen M. G., Groves B. A., Dopita M. A., Sutherland R. S., Kewley L. J., 2008, *The MAPPINGS III library of fast radiative shock models*, The Astrophysical Journal Supplement Series, 178, 20

Bacon R., et al., 2001, *The SAURON project–I. The panoramic integral-field spectrograph*, Monthly Notices of the Royal Astronomical Society, 326, 23

Baes M., 2019, *Panchromatic SED fitting codes and modelling techniques*, Proceedings of the International Astronomical Union, 15, 26–34

Baes M., Camps P., 2015, *SKIRT: The design of a suite of input models for Monte Carlo radiative transfer simulations*, Astronomy and Computing, 12, 33

Baes M., Verstappen J., De Looze I., Fritz J., Saftly W., Pérez E. V., Stalevski M., Valcke S., 2011, *Efficient three-dimensional NLTE dust radiative transfer with SKIRT*, The Astrophysical Journal Supplement Series, 196, 22

Bell E. F., McIntosh D. H., Katz N., Weinberg M. D., 2003, *The optical and near-infrared properties of galaxies. I. Luminosity and stellar mass functions*, The Astrophysical Journal Supplement Series, 149, 289

Bertelli G., Bressan A., Chiosi C., Fagotto F., Nasi E., 1994, *Theoretical isochrones from models with new radiative opacities*, Astronomy and Astrophysics Supplement Series, 106, 275

Bluck A. F. L., et al., 2020, *How do central and satellite galaxies quench? – Insights from spatially resolved spectroscopy in the MaNGA survey*, Monthly Notices of the Royal Astronomical Society, 499, 230

Bressan A., Marigo P., Girardi L., Salasnich B., Dal Cero C., Rubele S., Nanni A., 2012, *PARSEC: stellar tracks and isochrones with the PAdova and TRieste Stellar Evolution Code*, Monthly Notices of the Royal Astronomical Society, 427, 127

Brinchmann J., Charlot S., White S. D. M., Tremonti C., Kauffmann G., Heckman T., Brinkmann J., 2004, *The physical properties of star-forming galaxies in the low-redshift Universe*, , 351, 1151

Bruzual G., Charlot S., 2003, *Stellar population synthesis at the resolution of 2003*, , 344, 1000

Bruzual A., et al., 1983, *Spectral evolution of galaxies. I-Early-type systems*, The Astrophysical Journal, 273, 105

Bundy K., et al., 2014, *Overview of the SDSS-IV MaNGA survey: mapping nearby galaxies at apache point observatory*, The Astrophysical Journal, 798, 7

Burgarella D., Buat V., Iglesias-Páramo J., 2005, *Star formation and dust attenuation properties in galaxies from a statistical* *ultraviolet-to-far-infrared analysis*, Monthly Notices of the Royal Astronomical Society, 360, 1413

Byler N., Dalcanton J. J., Conroy C., Johnson B. D., 2017, *Nebular continuum and line emission in stellar population synthesis models*, The Astrophysical Journal, 840, 44

Calzetti D., Kinney A. L., Storchi-Bergmann T., 1994, *Dust extinction of the stellar continua in starburst galaxies: The ultraviolet and optical extinction law*, The astrophysical journal. Chicago. Vol. 429, no. 2, pt. 1 (July 1994), p. 582-601

Camps P., Baes M., 2015, *SKIRT: An advanced dust radiative transfer code with a user-friendly architecture*, Astronomy and Computing, 9, 20

Camps P., Baes M., 2020, *SKIRT 9: Redesigning an advanced dust radiative transfer code to allow kinematics, line transfer and polarization by aligned dust grains*, Astronomy and Computing, 31, 100381

Cardelli J. A., Clayton G. C., Mathis J. S., 1989, *The relationship between infrared, optical, and ultraviolet extinction*, Astrophysical Journal, Part 1 (ISSN 0004-637X), vol. 345, Oct. 1, 1989, p. 245-256., 345, 245

Carnall A. C., Leja J., Johnson B. D., McLure R. J., Dunlop J. S., Conroy C., 2019, *How to measure galaxy star formation histories. I. Parametric models*, The Astrophysical Journal, 873, 44

Chabrier G., 2003, *Galactic Stellar and Substellar Initial Mass Function*, , 115, 763

Choi J., Dotter A., Conroy C., Cantiello M., Paxton B., Johnson B. D., 2016, *Mesa isochrones and stellar tracks (MIST). I. Solar-scaled models*, The Astrophysical Journal, 823, 102

Conroy C., 2013, *Modeling the panchromatic spectral energy distributions of galaxies*, Annual Review of Astronomy and Astrophysics, 51, 393

Conroy C., Gunn J. E., White M., 2009, *The propagation of uncertainties in stellar population synthesis modeling. I. The relevance of uncertain aspects of stellar evolution and the initial mass function to the derived physical properties of galaxies*, The Astrophysical Journal, 699, 486

Conselice C. J., 2014, *The evolution of galaxy structure over cosmic time*, Annual Review of Astronomy and Astrophysics, 52, 291

Crain R. A., et al., 2015, *The EAGLE simulations of galaxy formation: calibration of subgrid physics and model variations*, Monthly Notices of the Royal Astronomical Society, 450, 1937

Davies J., et al., 2017, *DustPedia: a definitive study of cosmic dust in the local universe*, Publications of the Astronomical Society of the Pacific, 129, 044102

Dorfman R., 1979, *A formula for the Gini coefficient*, The review of economics and statistics, pp 146–149

Emami R., et al., 2021, *Morphological Types of DM Halos in Milky Way-like Galaxies in the TNG50 Simulation: Simple, Twisted, or Stretched*, The Astrophysical Journal, 913, 36

Engler C., et al., 2021, *The abundance of satellites around Milky Way-and M31-like galaxies with the TNG50 simulation: a matter of diversity*, Monthly Notices of the Royal Astronomical Society, 507, 4211

Falcón-Barroso J., Sánchez-Blázquez P., Vazdekis A., Ricciardelli E., Cardiel N., Cenarro A., Gorgas J., Peletier R., 2011, *An updated MILES stellar library and stellar population models*, Astronomy & Astrophysics, 532, A95

Ferland G. J., et al., 2017, *The 2017 Release Cloudy*, , 53, 385

Fernandes R. C., Mateus A., Sodré L., Stasińska G., Gomes J. M., 2005, *Semi-empirical analysis of Sloan Digital Sky Survey galaxies–I. Spectral synthesis method*, Monthly Notices of the Royal Astronomical Society, 358, 363

Fernandes R. C., et al., 2013a, *Resolving galaxies in time and space-I. Applying STARLIGHT to CALIFA datacubes*, Astronomy & Astrophysics, 557, A86

Fernandes R. C., et al., 2013b, *Resolving galaxies in time and space-I. Applying STARLIGHT to CALIFA datacubes*, Astronomy & Astrophysics, 557, A86

Fioc, Michel Rocca-Volmerange, Brigitte 2019, *PÉGASE.3: A code for modeling the UV-to-IR/submm spectral and chemical evolution of galaxies with dust*, A&A, 623, A143

Fritz J., et al., 2007, *A spectrophotometric model applied to cluster galaxies: the WINGS dataset*, Astronomy & Astrophysics, 470, 137

Fritz J., Poggianti B., Cava A., Moretti A., 2011, *Equivalent width Measurements in Optical Spectra of Galaxies in Local Clusters: Hints On the Star Formation History in Clusters*, Open Astronomy, 20

Fritz J., et al., 2017, *GASP. III. JO36: A Case of Multiple Environmental Effects at Play?*, The Astrophysical Journal, 848, 132

Goz D., Monaco P., Granato G. L., Murante G., Domínguez-Tenreiro R., Obreja A., Annunziatella M., Tescari E., 2017, *Panchromatic spectral energy distributions of simulated galaxies: results at redshift z = 0*, Monthly Notices of the Royal Astronomical Society

Grand R. J., et al., 2017, *The Auriga Project: the properties and formation mechanisms of disc galaxies across cosmic time*, Monthly Notices of the Royal Astronomical Society, 467, 179

Guedes J., Callegari S., Madau P., Mayer L., 2011, *Forming Realistic Late-type Spirals in a ΛCDM Universe: The Eris Simulation*, , 742, 76

Guidi G., et al., 2018, *The SELGIFS data challenge: generating synthetic observationsof CALIFA galaxies from hydrodynamical simulations*, Monthly Notices of the Royal Astronomical Society, 479

Hayward C. C., Smith D. J. B., 2014, *Should we believe the results of ultraviolet–millimetre galaxy spectral energy distribution modelling?*, Monthly Notices of the Royal Astronomical Society, 446, 1512

Hubble E., 1926, *No. 324. Extra-galactic nebulae.*, Contributions from the Mount Wilson Observatory / Carnegie Institution of Washington, 324, 1

Ibarra-Medel H. J., Avila-Reese V., Sánchez S. F., González-Samaniego A., Rodríguez-Puebla A., 2019, *Optical integral field spectroscopy observations applied to simulated galaxies: testing the fossil record method*, Monthly Notices of the Royal Astronomical Society, 483, 4525

Jacoby G. H., Hunter D. A., Christian C. A., 1984, *A library of stellar spectra.*, , 56, 257

Jain S., Tacchella S., Mosleh M., 2023, *The motivation for flexible star-formation histories from spatially resolved scales within galaxies*, Monthly Notices of the Royal Astronomical Society, p. stad3333

Jáquez-Domínguez J. M., et al., 2023, *Simulated observations of star formation regions: infrared evolution of globally collapsing clouds*, The Astrophysical Journal, 950, 88

Johnson B. D., Leja J., Conroy C., Speagle J. S., 2021, *Stellar Population Inference with Prospector*, , 254, 22

Jones A., Köhler M., Ysard N., Bocchio M., Verstraete L., 2017, *The global dust modelling framework THEMIS*, Astronomy & Astrophysics, 602, A46

Kapoor A. U., et al., 2021, *High-resolution synthetic UV–submm images for simulated Milky Way-type galaxies from the Auriga project*, Monthly Notices of the Royal Astronomical Society, 506, 5703

Kapoor A. U., et al., 2023, *TODDLERS: a new UV–mm emission library for star-forming regions–I. Integration with SKIRT and public release*, Monthly Notices of the Royal Astronomical Society, 526, 3871

Kaushal Y., et al., 2023, *A census of star formation histories of massive galaxies at 0.6< z< 1 from spectro-photometric modeling using Bagpipes and Prospector*, arXiv preprint arXiv:2307.03725

Kennicutt R. C. J., Evans N. J., 2012, *Star formation in the Milky Way and nearby galaxies*, Annual Review of Astronomy and Astrophysics, 50, 531

Kravtsov A. V., Klypin A. A., Khokhlov A. M., 1997, *Adaptive refinement tree: a new high-resolution N-body code for cosmological simulations*, The Astrophysical Journal Supplement Series, 111, 73

Kroupa P., 2002, *The Initial Mass Function of Stars: Evidence for Uniformity in Variable Systems*, Science, 295, 82

Lacerda E. A., Sánchez S., Mejía-Narváez A., Camps-Fariña A., Espinosa-Ponce C., Barrera-Ballesteros J., Ibarra-Medel H., Lugo-Aranda A., 2022, *pyPipe3D: Spectroscopy analysis pipeline*, Astrophysics Source Code Library, pp ascl–2206

Leitherer C., et al., 1999, *Starburst99: synthesis models for galaxies with active star formation*, The Astrophysical Journal Supplement Series, 123, 3

Leja J., Carnall A. C., Johnson B. D., Conroy C., Speagle J. S., 2019, *How to Measure Galaxy Star Formation Histories. II. Nonparametric Models*, The Astrophysical Journal, 876, 3

Longhetti M., Saracco P., 2009, *Stellar mass estimates in early-type galaxies: procedures, uncertainties and models dependence*, Monthly Notices of the Royal Astronomical Society, 394, 774

Lower S., Narayanan D., Leja J., Johnson B. D., Conroy C., Davé R., 2020, *How well can we measure the stellar mass of a galaxy: The impact of the assumed star formation history model in SED fitting*, The Astrophysical Journal, 904, 33

Madau P., Dickinson M., 2014, *Cosmic Star-Formation History*, , 52, 415

Madau P., Ferguson H. C., Dickinson M. E., Giavalisco M., Steidel C. C., Fruchter A., 1996, *High-redshift galaxies in the Hubble Deep Field: colour selection and star formation history to z∼4*, , 283, 1388

Madau P., Pozzetti L., Dickinson M., 1998, *The Star Formation History of Field Galaxies*, , 498, 106

Maraston C., 1998, *Evolutionary synthesis of stellar populations: a modular tool*, Monthly Notices of the Royal Astronomical Society, 300, 872

Maraston C., Strömbäck G., 2011, *Stellar population models at high spectral resolution*, Monthly Notices of the Royal Astronomical Society, 418, 2785

Maraston C., et al., 2020, *Stellar population models based on the SDSS-IV MaStar library of stellar spectra–I. Intermediate-age/old models*, Monthly Notices of the Royal Astronomical Society, 496, 2962

Marinacci F., et al., 2018, *First results from the IllustrisTNG simulations: radio haloes and magnetic fields*, Monthly Notices of the Royal Astronomical Society, 480, 5113

Mobasher B., et al., 2015, *A critical assessment of stellar mass measurement methods*, The Astrophysical Journal, 808, 101

Monceau-Baroux R., Keppens R., 2017, *Shock-cloud interaction and gas-dust spatial separation*, Astronomy & Astrophysics, 600, A134

Nagaraj G., Forbes J. C., Leja J., Foreman-Mackey D., Hayward C. C., 2022, *Empirical Dust Attenuation Model Leads to More Realistic UVJ Diagram for TNG100 Galaxies*, arXiv preprint arXiv:2204.06449

Nanni L., et al., 2022, *iMaNGA: mock MaNGA galaxies based on IllustrisTNG and MaStar SSPs–I. Construction and analysis of the mock data cubes*, Monthly Notices of the Royal Astronomical Society, 515, 320

Nanni L., et al., 2023, *iMaNGA: mock MaNGA galaxies based on IllustrisTNG and MaStar SSPs–II. The catalogue*, Monthly Notices of the Royal Astronomical Society, 522, 5479

Nelson D., et al., 2015, *The illustris simulation: Public data release*, Astronomy and Computing, 13, 12

Nelson D., et al., 2018, *First results from the IllustrisTNG simulations: the galaxy colour bimodality*, Monthly Notices of the Royal Astronomical Society, 475, 624

Pforr J., Maraston C., Tonini C., 2012, *Recovering galaxy stellar population properties from broad-band spectral energy distribution fitting*, Monthly Notices of the Royal Astronomical Society, 422, 3285

Pillepich A., et al., 2018, *First results from the IllustrisTNG simulations: the stellar mass content of groups and clusters of galaxies*, Monthly Notices of the Royal Astronomical Society, 475, 648

Pillepich A., et al., 2023, *Milky Way and Andromeda analogs from the TNG50 simulation*, arXiv preprint arXiv:2303.16217

Poggianti B. M., et al., 2017, *GASP. I. Gas stripping phenomena in galaxies with MUSE*, The Astrophysical Journal, 844, 48

Qin J., et al., 2022, *Systematic biases in determining dust attenuation curves through galaxy SED fitting*, Monthly Notices of the Royal Astronomical Society, 511, 765

Richard J., 2019, *A Blue MUSE for the VLT*, The Very Large Telescope in 2030, p. 24

Saftly W., Baes M., De Geyter G., Camps P., Renaud F., Guedes J., De Looze I., 2015, *Large and small-scale structures and the dust energy balance problem in spiral galaxies*, Astronomy & Astrophysics, 576, A31

Salpeter E. E., 1955, *The Luminosity Function and Stellar Evolution.*, , 121, 161

Sánchez S., et al., 2012, *Califa, the calar alto legacy integral field area survey-i. survey presentation*, Astronomy & Astrophysics, 538, A8

Sánchez S., Pérez E., et al., 2016, *Pipe3D, a pipeline to analyze integral field spectroscopy data: I. New fitting philosophy of FIT3D*, Revista mexicana de astronomía y astrofísica, 52, 21

Sánchez S., et al., 2022, *SDSS-IV MaNGA: pyPipe3D analysis release for 10,000 galaxies*, The Astrophysical Journal Supplement Series, 262, 36

Sarmiento R., Huertas-Company M., Knapen J. H., Ibarra-Medel H., Pillepich A., Sánchez S. F., Boecker A., 2022, *MaNGIA: 10,000 mock galaxies for stellar population analysis*

Sarmiento R., Knapen J. H., Ibarra-Medel H., Pillepich A., Sánchez S. F., Boecker A., et al., 2023, *MaNGIA: 10 000 mock galaxies for stellar population analysis*, Astronomy & Astrophysics, 673, A23

Sawicki M., Lin H., Yee H., 1996, *Evolution of the galaxy population based on photometric redshifts in the Hubble Deep Field*, arXiv preprint astro-ph/9610100

Smith D. J. B., Hayward C. C., 2018, *Panchromatic SED modelling of spatially resolved galaxies*, Monthly Notices of the Royal Astronomical Society, 476, 1705

Snyder G. F., et al., 2015, *Galaxy morphology and star formation in the Illustris Simulation at z= 0*, Monthly Notices of the Royal Astronomical Society, 454, 1886

Sodré L. J., Cuevas H., 1994, *Spectral classification of galaxies*, Vistas in Astronomy, 38, 287

Sorba R., Sawicki M., 2015, *Missing stellar mass in SED fitting: spatially unresolved photometry can underestimate galaxy masses*, Monthly Notices of the Royal Astronomical Society, 452, 235

Springel V., 2010, *E pur si muove: Galilean-invariant cosmological hydrodynamical simulations on a moving mesh*, Monthly Notices of the Royal Astronomical Society, 401, 791

Springel V., et al., 2018, *First results from the IllustrisTNG simulations: matter and galaxy clustering*, Monthly Notices of the Royal Astronomical Society, 475, 676

Stalevski M., Fritz J., Baes M., Nakos T., Popović L. Č., 2012, *3D radiative transfer modelling of the dusty tori around active galactic nuclei as a clumpy two-phase medium*, Monthly Notices of the Royal Astronomical Society, 420, 2756

Stalevski M., Tristram K. R., Asmus D., 2019, *Dissecting the active galactic nucleus in Circinus–II. A thin dusty disc and a polar outflow on parsec scales*, Monthly Notices of the Royal Astronomical Society, 484, 3334

Sánchez S. F., 2020, *Spatially Resolved Spectroscopic Properties of Low-Redshift Star-Forming Galaxies*, Annual Review of Astronomy and Astrophysics, 58, 99

Sánchez S. F., Rosales-Ortega F. F., Kennicutt R. C., Johnson B. D., Diaz A. I., Pasquali A., Hao C. N., 2010, *PPAK Wide-field Integral Field Spectroscopy of NGC 628 – I. The largest spectroscopic mosaic on a single galaxy**, Monthly Notices of the Royal Astronomical Society, 410, 313

Tinsley B., 1972, *Galactic evolution*, Astronomy and Astrophysics, 20, 383

Tojeiro R., Heavens A. F., Jimenez R., Panter B., 2007, *Recovering galaxy star formation and metallicity histories from spectra using VESPA*, Monthly Notices of the Royal Astronomical Society, 381, 1252

Torrey P., Vogelsberger M., Sijacki D., Springel V., Hernquist L., 2012, *Moving-mesh cosmology: properties of gas discs*, Monthly Notices of the Royal Astronomical Society, 427, 2224

Torrey P., et al., 2015, *Synthetic galaxy images and spectra from the Illustris simulation*, , 447, 2753

Torrey P., et al., 2019, *The evolution of the mass–metallicity relation and its scatter in IllustrisTNG*, Monthly Notices of the Royal Astronomical Society, 484, 5587

Trayford J. W., et al., 2017, *Optical colours and spectral indices of z= 0.1 eagle galaxies with the 3D dust radiative transfer code skirt*, Monthly Notices of the Royal Astronomical Society, 470, 771

Trčka A., et al., 2022, *UV to submillimetre luminosity functions of TNG50 galaxies*, Monthly Notices of the Royal Astronomical Society, 516, 3728

Vazdekis A., 1999, *Evolutionary stellar population synthesis at 2 Å spectral resolution*, The Astrophysical Journal, 513, 224

Villa-Vélez J., Buat V., Theulé P., Boquien M., Burgarella D., 2021, *Fitting spectral energy distributions of FMOS-COSMOS emission-line galaxies at z 1.6: Star formation rates, dust attenuation, and [OIII] λ5007 emission-line luminosities*, Astronomy & Astrophysics, 654, A153

Vogelsberger M., et al., 2014, *Introducing the Illustris Project: simulating the coevolution of dark and visible matter in the Universe*, Monthly Notices of the Royal Astronomical Society, 444, 1518

Vogelsberger M., et al., 2020, *High-redshift JWST predictions from IllustrisTNG: dust modelling and galaxy luminosity functions*, Monthly Notices of the Royal Astronomical Society, 492, 5167

Walcher J., Groves B., Budavári T., Dale D., 2011, *Fitting the integrated spectral energy distributions of galaxies*, Astrophysics and Space Science, 331, 1

Werle A., et al., 2022, *Post-starburst Galaxies in the Centers of Intermediate-redshift Clusters*, The Astrophysical Journal, 930, 43

Westera P., Buser R., 2003, in New Horizons in Globular Cluster Astronomy. p. 238

Wilkinson D. M., Maraston C., Goddard D., Thomas D., Parikh T., 2017, *FIREFLY (Fitting IteRativEly For Likelihood analYsis): a full spectral fitting code*, Monthly Notices of the Royal Astronomical Society, 472, 4297

Williams T. G., Baes M., De Looze I., Relaño M., Smith M. W. L., Verstocken S., Viaene S., 2019, *High-resolution radiative transfer modelling of M33*, Monthly Notices of the Royal Astronomical Society, 487, 2753

York D. G., et al., 2000, *The sloan digital sky survey: Technical summary*, The Astronomical Journal, 120, 1579

Yuan, Fang-Ting Argudo-Fernández, María Shen, Shiyin Hao, Lei Jiang, Chunyan Yin, Jun Boquien, Médéric Lin, Lihwai 2018, *Spatially resolved star formation and dust attenuation in Mrk 848: Comparison of the integral field spectra and the UV-to-IR SED*, A&A, 613, A13

Zana T., et al., 2022, *Morphological decomposition of TNG50 galaxies: methodology and catalogue*, Monthly Notices of the Royal Astronomical Society, 515, 1524

da Cunha E., Charlot S., Elbaz D., 2008, *A simple model to interpret the ultraviolet, optical and infrared emission from galaxies*, , 388, 1595

de Vaucouleurs G., 1959, *Classification and Morphology of External Galaxies.*, Handbuch der Physik, 53, 275